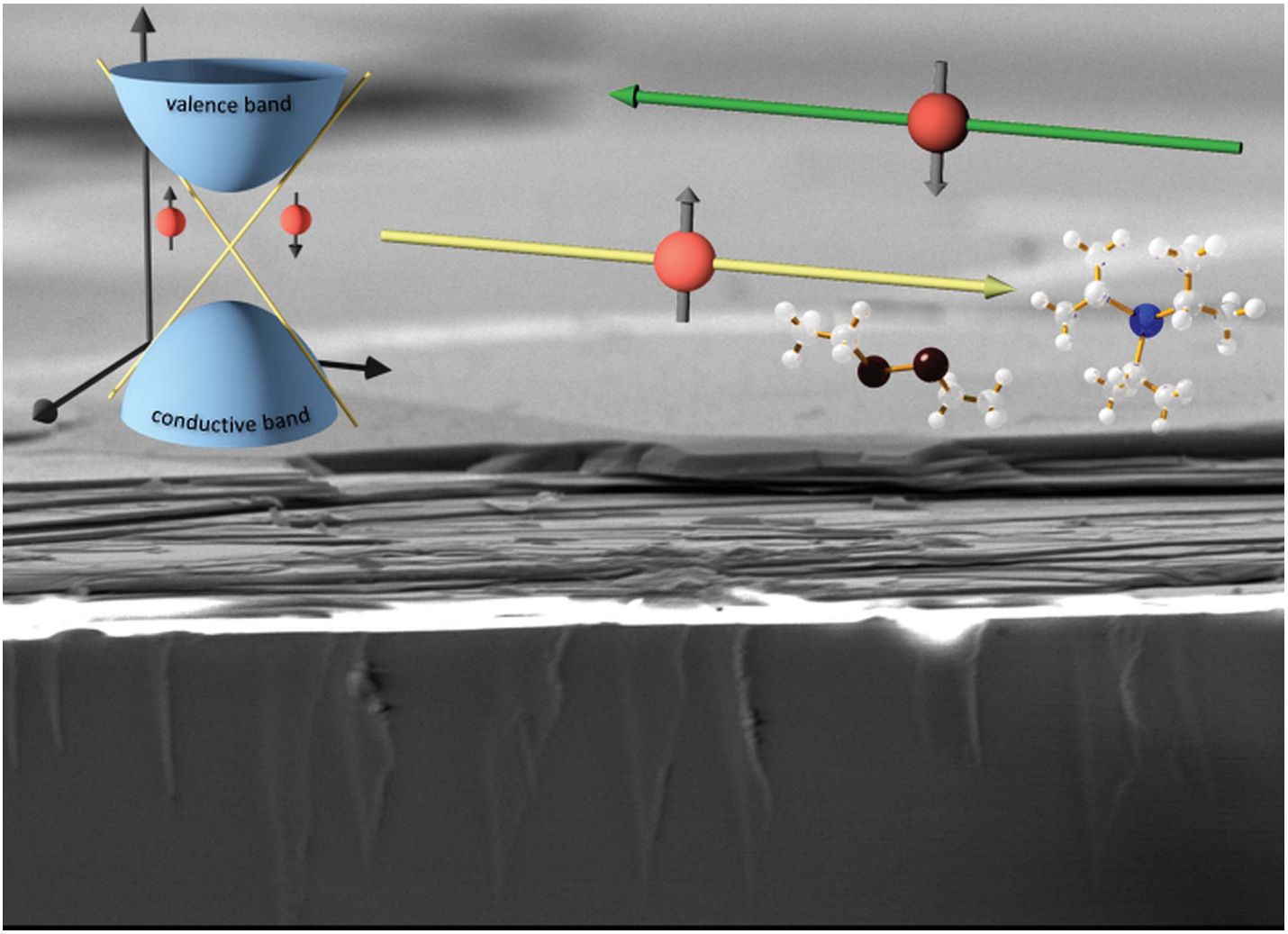

Showcasing the work on MOCVD-grown, epitaxial Sb_2Te_3 thin films presented by Prof. Stephan Schulz, Faculty of Chemistry, University of Duisburg-Essen and Center for Nanointegration Duisburg Essen (CENIDE).

Title: Deposition of topological insulator Sb_2Te_3 films by an MOCVD process

Smooth Sb_2Te_3 films were layer-by-layer grown on *c*-oriented Al_2O_3 substrates using Et_2Te_2 and i-Pr_3Sb. The high quality films allowed for the first time the measurement of the topological surface state for MOCVD grown Sb_2Te_3 by ARPES.

As featured in:

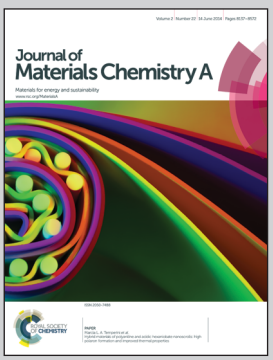

See Stephan Schulz *et al.*, *J. Mater. Chem. A*, 2014, **2**, 8215.

ROYAL SOCIETY OF CHEMISTRY

www.rsc.org/MaterialsA

Registered charity number: 207890

Journal of Materials Chemistry A

PAPER

View Article Online
View Journal | View Issue

Cite this: J. Mater. Chem. A, 2014, 2, 8215

Deposition of topological insulator Sb_2Te_3 films by an MOCVD process

Georg Bendt,[a] Sebastian Zastrow,[b] Kornelius Nielsch,[b] Partha Sarathi Mandal,[c] Jaime Sánchez-Barriga,[c] Oliver Rader[c] and Stephan Schulz*[a]

Received 10th February 2014
Accepted 11th March 2014

DOI: 10.1039/c4ta00707g

www.rsc.org/MaterialsA

Layered Sb_2Te_3 films were grown by a MOCVD process on Al_2O_3(0001) substrates at 400 °C by use of i-Pr_3Sb and Et_2Te_2 and characterized by SEM, AFM, XRD, EDX and Auger spectroscopy. The electrical sheet resistivity was measured in the range of 4 to 400 K, showing a monotonic increase with increasing temperature. The valence band structure probed by angle-resolved photoemission shows the detailed dispersions of the bulk valence band and the topological surface state of a quality no less than for optimized bulk single crystals. The surface state dispersion gives a Dirac point roughly 30 meV above the Fermi level leading to hole doping and the presence of bulk valence states at the Fermi energy.

Introduction

Antimony telluride (Sb_2Te_3) belongs to the class of V_2VI_3 layered materials (V = Sb, Bi; VI = S, Se, Te) with a tetradymite structure. Sb_2Te_3 has been investigated for quite a long time since it is a narrow band-gap (E_{gap} = 0.26 eV) semiconductor with good thermoelectric characteristics near room temperature.[1–3] More recently, the interest in Sb_2Te_3 increased due to its capability to serve as a topological insulator[4–6] with promising technical applications in spintronics and topological quantum computation.[7,8] Topological insulators are bulk insulators with metallic surfaces. They are characterized by a bulk band inversion and strong spin–orbit interaction which lead to surface states that bridge the bulk band gap. The surface states display a linear dispersion in the band structure and are protected by time-reversal symmetry.[7,8] The tetradymite binary compounds such as Bi_2Te_3, Bi_2Se_3, and Sb_2Te_3 are prototypical topological insulators while Sb_2Se_3 lacks a sufficiently strong spin–orbit interaction to develop the topological surface state, according to density functional theory.[9] Different from the theoretical predictions,[6] Bi_2Te_3 and Bi_2Se_3 are intrinsically electron doped with the Fermi energy (E_F) strongly displaced (≈0.3–0.4 eV) from the theoretical value so that it lies in the bulk conduction band and transport is expected to be bulk dominated. This strong electron doping does not occur for Sb_2Te_3,[10,11] rendering this material very promising for reaching the topological transport regime.

Sb_2Te_3 thin films were prepared in the past by microwave heating,[12,13] vapour phase transport,[14–21] vapour–liquid–solid growth,[22,23] atomic layer epitaxy,[24] electrochemical deposition,[25–31] DC and RF sputtering,[32,33] and molecular beam epitaxy (MBE).[34,35] Unfortunately, these processes very often only produced polycrystalline or highly faceted Sb_2Te_3 films, which additionally often suffered from high antisite concentrations, which typically result in a strong shift of the Fermi energy.

Metal organic chemical vapour deposition (MOCVD) is a promising technical alternative, which has been shown to produce crystalline Sb_2Te_3 films.[36–44] In MOCVD processes, trialkylstibines SbR_3 (R = Me, Et) and dialkyltellanes TeR_2' (R = Et, i-Pr, *t*-Bu) are typically used as molecular precursors.[45] Unfortunately, these precursors often require high pyrolysis temperatures, forcing the incorporation of impurities such as carbon into the material film. Therefore, there is a strong demand for alternative metal organic precursors. Single-source precursors are promising candidates for low-temperature deposition processes.[46] We recently demonstrated that $(Et_2Sb)_2Te$ can be used as an MOCVD precursor for the synthesis of highly stoichiometric Sb_2Te_3 films with very low antisite defect concentrations at temperatures as low as 200 °C,[47] while O'Brien *et al.* and Chivers *et al.* deposited Sb_2Te_3 films in the temperature range from 375 to 475 °C using $Sb[(TePi\text{-}Pr_2)_2N]_3$ in an aerosol-assisted chemical vapour deposition (AACVD) process.[48] Unfortunately, the Sb_2Te_3 films obtained with both precursors were rather polycrystalline, consisting of hexagonal Sb_2Te_3 nanoplates. In the case of the $(Et_2Sb)_2Te$ precursor, the low substrate temperature (200 °C) limited the diffusion mobility of the deposited Sb and Te atoms, hence avoiding the formation of a flat film. In contrast, higher substrate temperatures yielded flat Sb_2Te_3 films, but these were contaminated by elemental antimony.

We therefore became interested in suitable Sb- and Te-precursors for the MOCVD deposition at temperatures between

[a]Institute of Inorganic Chemistry and Center for Nanointegration Duisburg-Essen (CeNIDE), University of Duisburg-Essen, Universitätsstr. 5-7, 45117 Essen, Germany. E-mail: stephan.schulz@uni-due.de

[b]Institute of Applied Physics, University of Hamburg, Jungiusstr. 11, 20355 Hamburg, Germany

[c]Helmholtz-Zentrum Berlin für Materialien und Energie, Elektronenspeicherring BESSY II, Albert-Einstein-Str. 15, 12489 Berlin, Germany

350 and 400 °C and report herein on the MOCVD deposition of Sb_2Te_3 films using i-Pr_3Sb as the Sb-source and Et_2Te_2 as the Te-source. Both precursors are stable liquids at ambient temperature with a good volatility. i-Pr_3Sb has been used in the past for the CVD-deposition of $GeSb_2Te_4$ phase change materials,[49–51] whereas Et_2Te_2 has not been used as a CVD precursor, to date. To the best of our knowledge, dimethyl ditellane Me_2Te_2 is the only ditellane that has been used as a MOCVD-precursor, to date,[52,53] but it suffers from a relatively low vapour pressure. We carefully investigated the distinctive role of different substrates and substrate temperatures on the growth of the antimony telluride films, which were analyzed by energy dispersive X-ray analysis (EDX) and Auger spectroscopy, powder X-ray diffraction (XRD), scanning electron microscopy (SEM) and atomic force microscopy (AFM). Moreover, the electrical resistance of these films was determined by a Physical Property Measurement System (PPMS) in the range of 4 to 400 K and angle-resolved photoemission spectroscopy (ARPES) experiments revealed that the surface electronic structure presents a slightly hole-doped Dirac cone with photon-energy dependent photoemission intensity and a more surface localized surface state at higher binding energy. The measured doping level of the Dirac cone indicates that bulk valence states are present at the Fermi energy where they dominate the transport properties.

Experimental section

Materials

i-Pr_3Sb and Et_2Te_2 were prepared by literature methods.[54,55]

MOCVD deposition

MOCVD studies were performed in a cold-wall high-vacuum MOCVD reactor.[47] Sb_2Te_3 films were deposited on either Si(100) or Al_2O_3(0001) substrates at a working pressure of 10 mbar within 15 minutes. Si(100) substrates were previously degreased with acetone, treated with hydrofluoric acid and heated to 500 °C at 10^{-3} mbar for 1 hour in the reactor. Al_2O_3(0001) substrates were degreased with acetone and cleaned with a 3 : 1 mixture of sulphuric acid and phosphoric acid before use. The precursors were loaded into bubblers attached to the MOCVD-reactor under inert conditions (Ar) and the bubbler temperature was set to −5 °C (i-Pr_3Sb) and 20 °C (Et_2Te_2) throughout the experiment. Argon was used as the carrier gas (40 sccm Et_2Te_2, 5 sccm i-Pr_3Sb) and the precursor flow was controlled by use of a mass flow controller (MKS Instruments). After the film deposition was finished, the system was cooled to ambient temperature within 30 minutes under vacuum.

DSC analysis

A DSC 200 Phox (Netzsch Gerätebau) was used for differential scanning calorimetry (DSC) analysis.

X-ray analysis

XRD patterns were obtained using a Bruker D8 Advance powder diffractometer with Cu K_α radiation (λ: 1.5418 Å).

Surface-analysis

The surface morphology of the Sb_2Te_3-film was investigated by AFM using an AFM Veeco diInnova and by SEM using a Jeol JSM 6510 equipped with an energy dispersive X-ray spectroscopy (EDX) device (Bruker Quantax 400). A cross-sectional sample of the Sb_2Te_3 film was prepared by using a Jeol Cross-Section Polisher (IB-09010CP).

Auger spectroscopy

SAM/AES studies were carried out on a Perkin Elmer PHI 660 Scanning Auger Microprobe System.

Photoelectron spectroscopy

Angle-resolved photoelectron spectroscopy (ARPES) was performed with linearly polarized synchrotron radiation (s + p) at the UE112-PGM2a undulator beamline of BESSY II using a Scienta R8000 hemispherical electron energy analyzer. The samples were transferred in air and the surface was prepared *in situ* by sputtering for 1 h at 1.5 keV at 1.2×10^{-5} mbar Ar pressure followed by 30 min annealing at 230 °C. ARPES was subsequently performed in a base pressure of 2×10^{-10} mbar at ambient temperature.

Results and discussion

Ditellanes R_2Te_2 are promising low-temperature Te precursors for MOCVD deposition due to their low thermal stability. Me_2Te_2, whose decomposition temperature is ≈100 °C lower compared to that of Me_2Te, has been successfully used by Kisker *et al.* for the growth of CdTe films at 250 °C.[56] Moreover, ditellanes are easily accessible by reaction of Na_2Te_2 with alkyl halides in liquid ammonia or other standard reactions.[57–59]

The thermal properties of Et_2Te_2 and i-Pr_3Sb were investigated by DSC to identify suitable substrate temperatures for the MOCVD process. The decomposition temperature of i-Pr_3Sb (255 °C) is significantly lower compared to that of Et_3Sb (310 °C) and Me_3Sb (370 °C), which are typically used for the MOCVD process (Fig. 1). Et_2Te_2 starts to disproportionate at 150 °C with subsequent formation of elemental tellurium and Et_2Te, which then decomposes at higher temperature (260 °C) as is shown by comparing the DSC curves of Et_2Te_2 (Fig. 2, black curve) and of pure Et_2Te (Fig. 2, red curve).

Sb_2Te_3 films were grown on polycrystalline Al_2O_3(0001) substrates at substrate temperatures between 350 and 400 °C using a home-made MOCVD cold-wall reactor and a deposition time of 15 minutes. An almost linear increasing growth rate with increasing substrate temperature was found in the temperature range from 350 °C to 400 °C, reaching 750 nm in 15 min at 400 °C. These findings point to a kinetically-controlled growth process, which we have also recently reported for the MOCVD deposition of Sb_2Te_3 films using $(Et_2Sb)_2Te$ as a single source precursor.[56] The chemical composition (EDX) and the crystallinity (XRD) of the resulting Sb_2Te_3 films were not affected by the increasing substrate temperature, whereas the morphology of the Sb_2Te_3 films changed significantly. Sb_2Te_3 films deposited at 350 °C (Fig. 3a) and 375 °C (Fig. 3b) show a

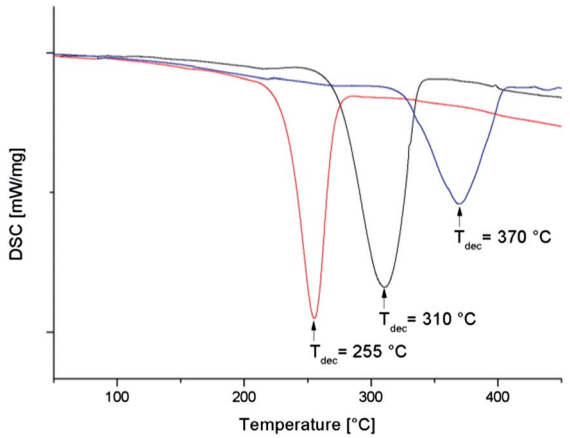

Fig. 1 DSC curves of i-Pr_3Sb (red curve), Et_3Sb (black curve) and Me_3Sb (blue curve).

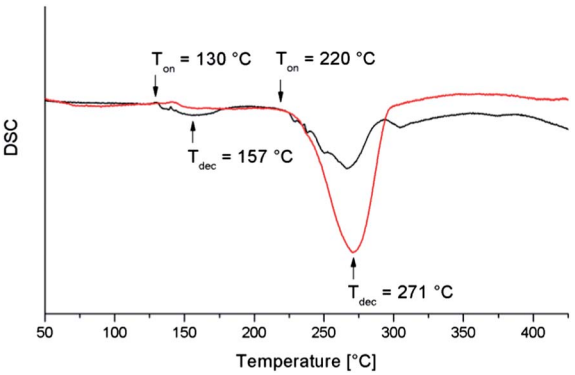

Fig. 2 DSC curves of Et_2Te_2 (black curve) and Et_2Te (red curve).

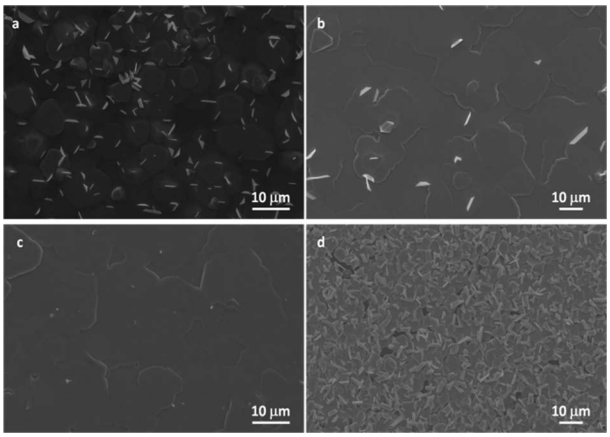

Fig. 3 SEM images of the Sb_2Te_3 film deposited at 350 °C (a), 375 °C (b) and 400 °C (c) on Al_2O_3(0001) and on Si(100) (d) substrates.

polycrystalline surface, most likely resulting from the low diffusion rates of adatoms as was observed with $(Et_2Sb)_2Te$.[47] In contrast, very smooth Sb_2Te_3 films were obtained at 400 °C (Fig. 3c). The substrate material also has a distinguished influence on the film morphology since the deposition on Si(100) substrates at 400 °C only yielded polycrystalline Sb_2Te_3 films (Fig. 3d).

The substrate typically affects the morphology of the growing film. Epitaxial films are preferentially grown on substrates which exhibit a small lattice mismatch (<7%) in order to reduce the lattice strain (so-called hetero-epitaxy).[60] However, since Sb_2Te_3 adopts a rhombohedral crystal structure, in which five monoatomic sheets in a sequence of Te–Sb–Te–Sb–Te are bonded in the *c*-axis direction, the Sb_2Te_3 films are always Te-terminated due to the weak van der Waals Te–Te bond. As a consequence, epitaxial V_2VI_3 films such as Sb_2Te_3, Bi_2Se_3 or Bi_2Te_3 have been grown on substrates with large lattice mismatches such as GaAs, Si(111) and Al_2O_3(0001), respectively, since the merely attached Sb_2Te_3 epilayers can achieve their own lattice parameters from the beginning of the growth.[61] This growth mechanism is typically referred to as van der Waals epitaxy,[62] which explains the formation of epitaxial Sb_2Te_3 films on Al_2O_3(0001). In contrast, Sb_2Te_3 films obtained on Si(100) always showed Sb_2Te_3 nanodisks of hexagonal shape perpendicular to the surface (Fig. 3d). Comparable findings were previously reported for Bi_2Se_3 films grown on Si(001).[63] The authors suggested that generating the nanodisks on the Bi_2Se_3 film is energetically more favorable than thickening the film.

Wang *et al.* showed that the substrate temperature is a key parameter for the MBE growth of high quality Sb_2Te_3 films on Al_2O_3(0001) substrates,[60] since both the reaction rate and the reaction kinetics are strongly influenced. The composition and surface morphology of the Sb_2Te_3 films was found to strongly depend on the substrate temperature. High-quality MBE grown films were obtained at 330 °C, whereas lower substrate temperatures gave Sb-deficient films due to the higher sticking coefficient of Te at low temperatures compared to that of Sb. Since the sticking coefficient of Te decreases at higher substrate temperatures, stoichiometric Sb_2Te_3 films were formed. However, Periano *et al.* also reported on the MBE growth of stoichiometric Sb_2Te_3 films at a substrate temperature of 250 °C.[64] Herein, we deposited highly stoichiometric Sb_2Te_3 films at 350 °C and at 400 °C. The film obtained at 400 °C is very flat, consisting of large Sb_2Te_3 flakes, whereas that obtained at 350 °C also showed hexagonal Sb_2Te_3 nanocrystals, which adopt orientations perpendicular to the film surface. The higher substrate temperature not only influences the decomposition kinetics of the precursor molecules, resulting in higher decomposition rates, but also affects the mobility of the adatoms, which increases with increasing substrate temperature, yielding larger Sb_2Te_3 nanoflakes. Moreover, the surface morphology (flatness) of the film improved with the increasing substrate temperature.

SEM (Fig. 4) and AFM micrographs (Fig. 5) of the Sb_2Te_3 film deposited on Al_2O_3(0001) substrates at 400 °C within 15 minutes prove the formation of smooth Sb_2Te_3 films over a large range (substrate dims. 10 × 10 mm). These results were confirmed by cross-sectional SEM microscopy (Fig. 5), showing a uniformly grown Sb_2Te_3 film of about 750 nm thickness.

The AFM micrograph (Fig. 6) shows regular terraces of 1 nm height, which correspond to one quintuple layer of the layered tetradymite-type structure of Sb_2Te_3.[65] These findings indicate a layered growth as was also observed in MBE-grown Sb_2Te_3 thin

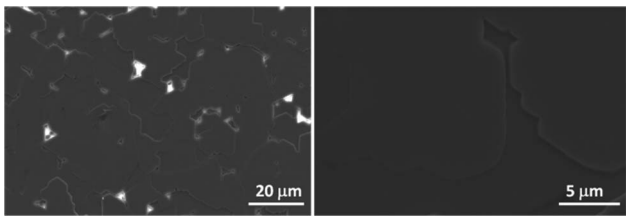

Fig. 4 SEM images of the Sb_2Te_3 film deposited at 400 °C on Al_2O_3(0001). Bright spots result from small holes in the film.

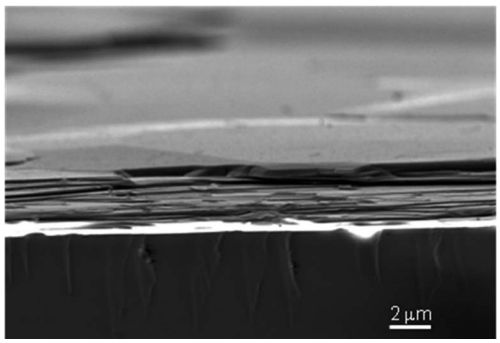

Fig. 5 Cross-sectional SEM image of a Sb_2Te_3 film deposited at 400 °C on an Al_2O_3(0001) substrate showing the layered structure of the Sb_2Te_3 film. The substrate orientation is tilted by about 15°.

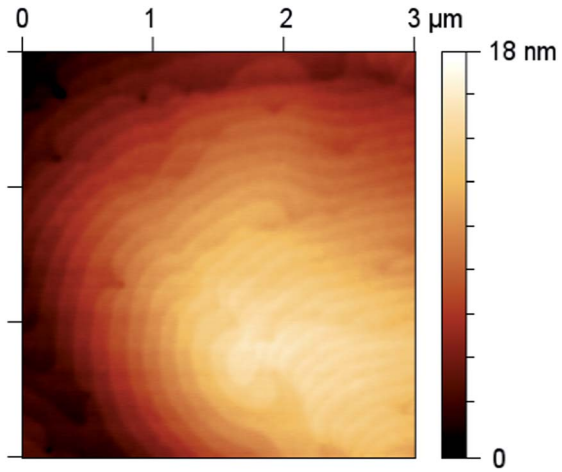

Fig. 6 AFM photograph of a Sb_2Te_3 film deposited at 400 °C on an Al_2O_3(0001) substrate.

films.[66] Sb_2Te_3 crystallizes in the space group $R\bar{3}m$-D_{3d}^5 and forms a layered, rhombohedral crystal structure.[67] It is built of anisotropic layers, in which five atomic planes are covalently bonded to the quintuple layer, that is roughly 1 nm thick and consists of five mono-atomic planes of Te(1)–Sb–Te(2)–Sb–Te(1) with 1 and 2 designating the different positions within the fivefold layer. The conventional unit cell includes three quintuple layers, which are bound by weak van der Waals forces.

The chemical composition of the material film was analyzed by EDX analysis. Almost perfect Sb_2Te_3 films with the expected 40 : 60 (Sb : Te) molar ratios were found (standard deviation ±0.5 (Sb) and ±1.0 (Te)). Fig. 7 shows an Sb_2Te_3-film at an early stage of growth. The SEM image shows single plates which are not fully coalesced. The corresponding element mapping by scanning Auger electron microscopy (SAES) shows a homogeneous distribution of Sb and Te within the Sb_2Te_3 plates. In addition, some carbon impurities are located between the Sb_2Te_3 plates on the substrate surface.

The X-ray diffractogram (XRD) of the Sb_2Te_3 film deposited at 400 °C (Fig. 8) clearly proved the formation of highly crystalline Sb_2Te_3 films. All reflection peaks can be indexed on the basis of the structure of rhombohedral Sb_2Te_3. In addition, a small reflex of the Al_2O_3(0001) substrate is visible at 41.6°. The peaks in the diffractogram correspond to (001) planes, pointing to a *c*-axis oriented growth as was previously reported for Sb_2Te_3 films grown by MBE,[68–70] and MOCVD,[40–42] respectively.

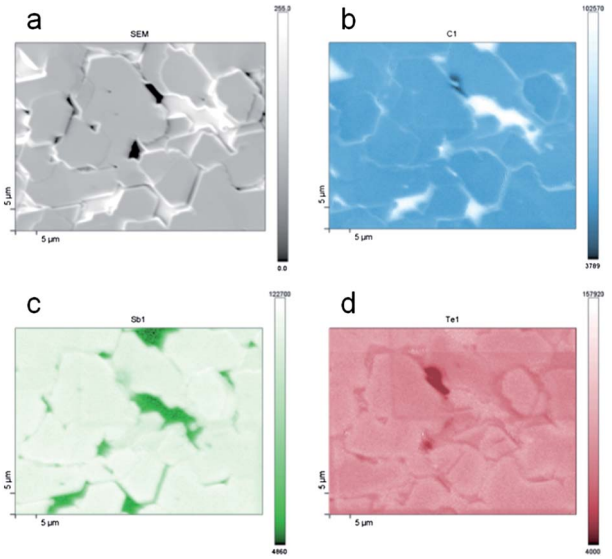

Fig. 7 SEM (a) and SAES study (mapping of C (b), Sb (c) and Te (d)) of an Sb_2Te_3 film deposited at 400 °C on (0001) Al_2O_3 substrates; high element concentrations are indicated by bright colour.

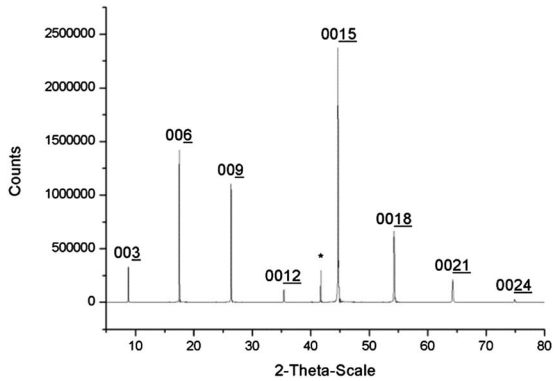

Fig. 8 2θ XRD pattern of the Sb_2Te_3 film deposited at 400 °C on an Al_2O_3(0001) substrate; peaks are labelled (JCPDS-ICDD card 15-0874); the asterisk (*) corresponds to the Al_2O_3(0001) substrate.

We have characterized the band structure of the surface by photoelectron spectroscopy (PES) after transfer to the photoelectron spectrometer and *in situ* preparation. To the best of our knowledge, this is the first time that angle-resolved photoemission spectroscopy (ARPES) studies have been performed on MOCVD-grown Sb_2Te_3 thin films. The PE spectrum in Fig. 9 shows Sb and Te core-levels without any shifted components similar to that of Bi_2Se_3.[71]

The overview ARPES spectra of the valence band in Fig. 10 show intense structures around 0.8 eV binding energy and more faint features near E_F which are well discernible at 16 and 17 eV photon energy but not at 21 eV, where their photoemission intensity is weak due to final state effects. Fig. 11 shows, therefore, the range near E_F for photon energies from 16 to 18 eV displaying the topological surface state. This surface state has previously been studied theoretically[9] and in ARPES experiments at selected photon energies (21.2 eV),[10,72] 55 eV,[11] 8.44 and 24 eV,[72] respectively.

While experiments on cleaved bulk samples led to the conclusion that the Fermi level does not cut the surface state,[73] epitaxial Sb_2Te_3/Si(111) films observed slight hole doping (Dirac point ≈100 meV above E_F) and, after deposition of 0.1 monolayer Cs, the undoped state with the Dirac point at E_F. The spin texture of the surface state has been probed by spin- and angle-resolved photoemission, and an additional, topologically protected, Rashba-split surface state was found.[11] These results have been confirmed recently for epitaxial Sb_2Te_3/Si(111) films.[72] In Fig. 10, this additional surface state is marked at 0.4–0.8 eV binding energy in the data taken at 21 eV photon energy. Due to its high binding energy, it does not contribute to transport. On the other hand it has been found to be much more surface localized than the topological surface state that forms the Dirac cone and its sharp, intense dispersing photoemission features here indicate the presence of a well ordered and stoichiometric surface.

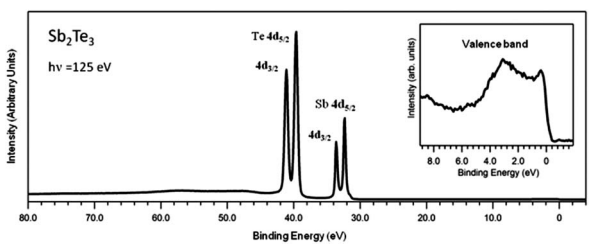

Fig. 9 Core-level photoemission characterization of the *in situ* prepared surface. Satellite peaks are not observed.

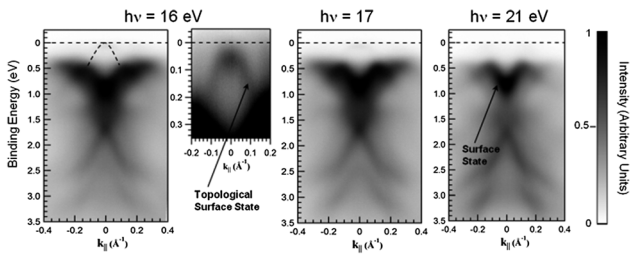

Fig. 10 Overview ARPES spectra of the valence band. The topological surface state forming a Dirac cone near the Fermi level (0 eV binding energy) is best observed at 16 eV photon energy. Another surface state with massive character appears as the higher binding energy and is best seen at 21 eV.

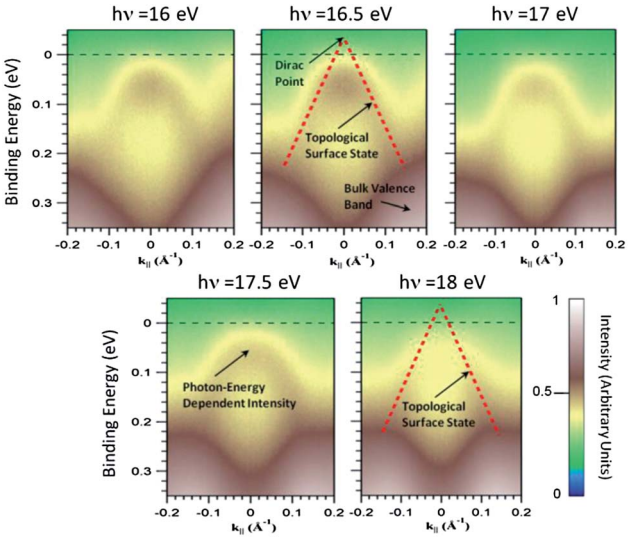

Fig. 11 Magnified spectra on the dependence of the topological surface state (Dirac cone) on the photon energy. The dashed line is a linear fit to the data at 16.5 eV and results in a Dirac point ≈30 meV above the Fermi level (hole doping). This Fermi level position means bulk transport according to band structure calculations.

Changing the photon energy in ARPES allows us principally to vary the perpendicular component of the electron wave vector, $\mathbf{k}_z$.[74] In this way, we can distinguish three-dimensional dispersing features from two-dimensional features. The identical *E vs.* $\mathbf{k}_{||}$ dispersion in Fig. 11 proves the two-dimensional character. The intensity, however, is subject to the $\mathbf{k}_z$-dependence of the parent bulk band structure, and this is seen at 18 eV as a shift of maximum intensity so that at 22 eV (not shown) the surface state is not discernible any longer. The intensity seen near the Fermi energy at 16 eV moves with increasing photon energy to lower binding energy and has crossed E_F at 18 eV. This intensity stems directly from bulk valence band states which exist in the complete lower Dirac cone up to the Dirac point as is evident from, *e.g.*, surface-projected bulk band calculations.[11] Due to these states, the topological transport regime will require the Fermi level to be in the upper Dirac cone. The linear dispersion predicted by theory has been fitted to the data at 16.5 eV in Fig. 11. Extrapolation of the data yields a Fermi velocity of $(2.72 \pm 0.14) \times 10^5$ m s^{-1}, roughly in agreement with previous measurements from single crystals [$(3.8 \pm 0.2) \times 10^5$ m s^{-1}] and density functional theory (3.2×10^5 m s^{-1}),[11] and a Dirac point ≈30 meV above E_F. The surface is, therefore, slightly hole doped. The calculation shows that bulk valence band states reach up to the Dirac point so that hole doping indicates that the Fermi level cuts through bulk valence band states rendering the transport bulk like.[11]

Electrical measurements were performed with a PPMS-system (DynaCool QuantumDesign) using the standard

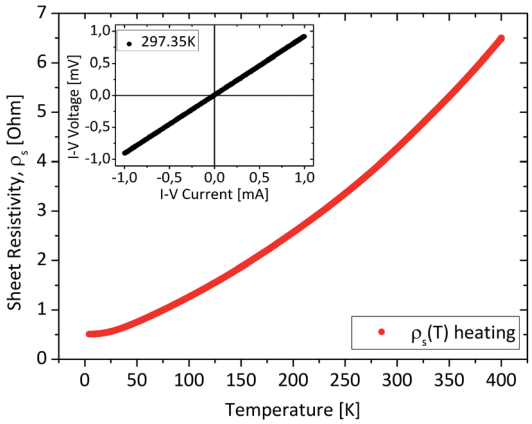

Fig. 12 Resistivity against temperature. The inset graph shows the *I*–*V*-curve measured at room temperature with 1 mA at 12.2 Hz.

Electronic Transport Option. By applying an alternate current of 1 mA with a frequency of 12.2 Hz and a sampling rate of 0.5 s^{-1}, the resistance was measured in the range of 4 to 400 K with a heating rate of 10 K min^{-1}. By making equally spaced 4-point contacts and choosing the contact spacing much larger than the film thickness, the sheet resistivity can be calculated by the following equation:[75]

$$\rho = \frac{\pi}{\ln 2}\frac{V}{I}.$$

I is the applied current at the outer contacts and *V* is the measured voltage drop between the inner contacts.

The measured sheet resistivity (Fig. 12) shows a metallic like behaviour with a dominating contribution of the carrier transport in the bulk, and a monotonic increase with increasing temperature as was previously observed for ALD-grown Sb_2Te_3 thin films.[24] Here the sheet resistance increases by one order of magnitude (10×) over the temperature range from 2 to 400 K, whereas the resistance of the ALD film increased moderately by the factor of 1.5 over the same temperature range. The MOCVD films exhibit a higher carrier concentration (>10^{19} cm^{-3}) correlated with intrinsic defects, most likely antisite defects as is common for Sb_2Te_3. Furthermore, we assume that the carrier concentration is nearly constant over the complete temperature range and the strong enhancement of the resistance over temperature is related to the reduction of the carrier mobility. Due to the high doping concentration the enhancement of the carrier concentration by thermal excitation of carriers over the bulk-bandgap is not observed by the resistance curve (Fig. 12) or has a negligible impact. In the case of ALD grown Sb_2Te_3 films a stabilisation of the resistance at least around 350 K has been reported.[24]

Conclusions

The layer-by-layer MOCVD deposition of highly crystalline Sb_2Te_3 films was achieved at substrate temperatures between 350 and 400 °C using i-Pr_3Sb and Et_2Te_2. Even though both precursors start to decompose at lower temperatures as was shown by DSC, higher temperatures are necessary in order to produce smooth and crystalline Sb_2Te_3 films. The film growth occurs under kinetic control, reaching deposition rates as high as 3 μm per hour at 400 °C. The electrical sheet resistivity was found to monotonically increase with increasing temperature. ARPES measurements for the first time showed the detailed dispersions of the bulk valence band and the topological surface state for MOCVD grown Sb_2Te_3 films with a quality no less than for optimized bulk single crystals. The surface state dispersion gives a Dirac point roughly 30 meV above the Fermi level leading to hole doping and the presence of bulk valence states at the Fermi energy. Additional Bi doping of the Sb_2Te_3 films is currently under investigation in order to further modify the valence band and the topological surface states.

Acknowledgements

Stephan Schulz (StS), Oliver Rader (OR) and Kornelius Nielsch (KN) acknowledge financial support by the DFG (priority program SPP 1666), the University of Duisburg-Essen (StS), the Karl-Vossloh-Stiftung (KN), and the University of Hamburg (KN). Partha Sarathi Mandal is supported by the Impuls- und Vernetzungsfonds der Helmholtz-Gemeinschaft. The authors like to thank PD Dr Nils Hartmann, University of Duisburg-Essen, for SAES studies.

Notes and references

1 R. Venkatasubramanian, E. Siivola, T. Colpitts and B. O'Quinn, *Nature*, 2001, **413**, 597.
2 T. C. Harman, P. J. Taylor, M. P. Walsh and B. E. LaForge, *Science*, 2002, **297**, 2229.
3 D. Hsieh, Y. Xia, D. Qian, L. Wray, F. Meier, J. H. Dil, J. Osterwalder, L. Patthey, A. V. Fedorov, H. Lin, A. Bansil, D. Grauer, Y. S. Hor, R. J. Cava and M. Z. Hasan, *Phys. Rev. Lett.*, 2009, **103**, 146401.
4 H. Zhang, C.-X. Liu, X.-L. Qi, X. Dai, Z. Fang and S.-C. Zhang, *Nat. Phys.*, 2009, **5**, 438.
5 L. He, X. Kou and K. L. Wang, *Phys. Status Solidi RRL*, 2013, **7**, 50.
6 J. J. Cha, K. J. Koski and Y. Cui, *Phys. Status Solidi RRL*, 2013, **7**, 15.
7 J. Moore, *Nat. Phys.*, 2009, **5**, 378.
8 X.-L. Qi, R. Li, J. Zang and S.-C. Zhang, *Science*, 2009, **323**, 1184.
9 H. Zhang, C.-X. Liu, X.-L. Qi, X. Dai, Z. Fang and S.-C. Zhang, *Nat. Phys.*, 2009, **5**, 438.
10 G. Wang, X. Zhu, J. Wen, X. Chen, K. He, L. Wang, X. Ma, Y. Liu, X. Dai, Z. Fang, J. Jia and Q. Xue, *Nano Res.*, 2010, **3**, 874.
11 C. Pauly, G. Bihlmayer, M. Liebmann, M. Grob, A. Georgi, D. Subramaniam, M. R. Scholz, J. Sánchez-Barriga, A. Varykhalov, S. Blügel, O. Rader and M. Morgenstern, *Phys. Rev. B: Condens. Matter Mater. Phys.*, 2012, **86**, 235106.

12 B. Zhou, Y. Ji, Y. F. Yang, X. H. Li and J. H. Zhu, *Cryst. Growth Des.*, 2008, **8**, 4394.
13 G.-H. Dong, Y.-J. Zhu and L.-D. Chen, *CrystEngComm*, 2011, **13**, 6811.
14 J. Chen, T. Sun, D. H. Sim, H. Peng, H. Wang, S. Fan, H. H. Hng, J. Ma, F. Y. C. Boey, S. Li, M. K. Samani, G. C. K. Chen, X. Chen, T. Wu and Q. Yan, *Chem. Mater.*, 2010, **22**, 3086.
15 L. M. Goncalves, C. Couto, P. Alpuim, D. M. Rowe and J. H. Correia, *Mater. Sci. Forum*, 2006, **514–516**, 156.
16 B. Lv, S. Hu, W. Li, X. Di, L. Feng, J. Zhang, L. Wu, Y. Cai, B. Li and Z. Lei, *Int. J. Photoenergy*, 2010, 476589, DOI: 10.1155/2010/476589.
17 A. M. Farid, H. E. Atyia and N. A. Hegab, *Vacuum*, 2005, **80**, 284.
18 K. Ulutas, D. Deger and S. Yakut, *J. Phys.: Conf. Ser.*, 2013, **417**, 012040.
19 G. Hao, X. Qi, G. Wang, X. Peng, S. Chang, X. Wei and J. Zhong, *RSC Adv.*, 2012, **2**, 10694.
20 G. Hao, X. Qi, Y. Fan, L. Xue, X. Peng, X. Wei and J. Zhong, *Appl. Phys. Lett.*, 2013, **102**, 013105.
21 L. M. Goncalves, P. Alpuim, A. G. Rolo and J. H. Correia, *Thin Solid Films*, 2011, **519**, 4152.
22 S. Meister, H. Peng, K. Mcllwrath, K. Jarausch, X. Zhang and F. Y. Cui, *Nano Lett.*, 2006, **6**, 1514.
23 J. S. Lee, S. Brittman, D. Yu and H. Park, *J. Am. Chem. Soc.*, 2008, **130**, 6252.
24 S. Zastrow, J. Gooth, T. Boehnert, S. Heiderich, W. Toellner, S. Heimann, S. Schulz and K. Nielsch, *Semicond. Sci. Technol.*, 2013, **28**, 035010.
25 Q. Huang, A. J. Kellock and S. Raoux, *J. Electrochem. Soc.*, 2008, **155**, D104.
26 M. Y. Kim, K. W. Park and T. S. Oh, *J. Korean Phys. Soc.*, 2008, **53**, 266.
27 D. Pinisetty, M. Gupta, A. B. Karki, D. P. Young and R. V. Devireddy, *J. Mater. Chem.*, 2011, **21**, 4098.
28 I. Y. Erdogan and U. Demir, *J. Electroanal. Chem.*, 2009, **633**, 253.
29 I.-J. Yoo, Y. Song, D. Chan Lim, N. V. Myung, K. Hyoung Lee, M. Oh, D. Lee, Y. Do Kim, S. Kim, Y.-H. Choa, J. Yul Lee, K. Hwan Lee and J.-H. Lim, *J. Mater. Chem. A*, 2013, **1**, 5430.
30 J.-H. Lim, M. Yeong Park, D.-C. Lim, N. V. Myung, J.-H. Lee, Y.-K. Jeong, B. Yoo and K. Hwan Lee, *Mater. Res. Bull.*, 2012, **47**, 2748.
31 J.-H. Lim, M. Yeong Park, D.-C. Lim, B. Yoo, J.-H. Lee, N. V. Myung and K. Hwan Lee, *J. Electron. Mater.*, 2011, **40**, 1321.
32 T. Chen, P. Fan, Z. Zheng, D. Zhang, X. Cai, G. Liang and Z. Cai, *J. Electron. Mater.*, 2012, **41**, 679.
33 B. Fang, Z. Zeng, X. Yan and Z. Hu, *J. Mater. Sci.: Mater. Electron.*, 2013, **24**, 1105.
34 N. Peranio, M. Winkler, D. Bessas, Z. Aabdin, J. Koenig, H. Böttner, R. P. Hermann and O. Eibl, *J. Alloys Compd.*, 2012, **521**, 163.
35 G. Wang, X. Zhu, J. Wen, X. Chen, K. He, L. Wang, X. Ma, Y. Liu, X. Dai, Z. Fang, J. Jia and Q. Xue, *Nano Res.*, 2010, **3**, 874.
36 T. J. Groshens, Jr, R. W. Gedridge and C. K. Lowe-Ma, *Chem. Mater.*, 1994, **6**, 727.
37 R. Venkatasubramanian, T. Colpitts, E. Watko, M. Lamvik and N. El-Masry, *J. Cryst. Growth*, 1997, **170**, 817.
38 B. Aboulfarah, A. Mzerd, A. Boulouz, A. Giani, A. Foucaran and A. Boyer, *Moroccan J. Condens. Matter*, 1998, **1**, 100.
39 A. Giani, A. Boulouz, F. Pascal-Delannoy, A. Foucaran, E. Charles and A. Boyer, *Mater. Sci. Eng., B*, 1998, **64**, 19.
40 R. Venkatasubramanian, T. Colpitts, B. O'Quinn, S. Liu, N. El-Masry and M. Lamvik, *Appl. Phys. Lett.*, 1999, **75**, 1104.
41 A. Giani, A. Boulouz, F. P. Delannoy, A. Foucaran, A. Boyer, B. Aboulfarah and A. Mzerd, *J. Mater. Sci. Lett.*, 1999, **18**, 541.
42 J. H. Kim, Y. C. Jung, S. H. Suh and J. S. Kim, *J. Nanosci. Nanotechnol.*, 2006, **6**, 3325.
43 J.-H. Kim, S.-D. Kwon, D.-Y. Jeong, B.-K. Ju, S.-J. Yoon and J.-S. Kim, *25th Internat. Conf. on Thermoelectrics, 2006 (ICT '06)*, pp. 411–413. DOI: 10.1109/ict.2006.331284.
44 J. S. Lee, S. Brittman, D. Yu and H. Park, *J. Am. Chem. Soc.*, 2008, **130**, 6252.
45 H. B. Singh and N. Sudha, *Polyhedron*, 1996, **15**, 745.
46 J. S. Ritch, T. Chivers, M. Afzaal and P. O'Brien, *Chem. Soc. Rev.*, 2007, **36**, 1622.
47 G. Bendt, S. Schulz, S. Zastrow and K. Nielsch, *Chem. Vap. Deposition*, 2013, **19**, 235.
48 S. S. Garje, D. J. Eisler, J. S. Ritch, M. Afzaal, P. O'Brien and T. Chivers, *J. Am. Chem. Soc.*, 2006, **128**, 3120.
49 R.-Y. Kim, H.-G. Kim, K.-W. Park, J.-K. Ahn and S.-G. Yoon, *Chem. Vap. Deposition*, 2009, **15**, 296.
50 R.-Y. Kim, H.-G. Kim and S.-G. Yoon, *J. Appl. Phys.*, 2007, **102**, 083531.
51 R.-Y. Kim, H.-G. Kim and S.-G. Yoon, *Appl. Phys. Lett.*, 2006, **89**, 102107.
52 D. W. Kisker, M. L. Steigerwald, T. Y. Kometani and K. S. Jeffers, *Appl. Phys. Lett.*, 1987, **50**, 1681.
53 W. M. Li, C. Y. Chen and R. M. Cohen, *J. Cryst. Growth*, 1995, **156**, 343.
54 M. Wieber, Sb Organoantimony Compounds Part 1, in *Gmelin Handbook of Inorganic Chemistry*, ed. H. Bitterer, Springer Verlag, Berlin, 8th edn, 1981.
55 K. Hamada and H. Morishita, *Synth. React. Inorg. Met.-Org. Chem.*, 1981, **11**, 597.
56 D. W. Kisker, M. L. Steigerwald, T. Y. Kometani and K. S. Jeffers, *Appl. Phys. Lett.*, 1987, **50**, 1681.
57 K. J. Irgolic, Organotellurium Compounds, in *Houben-Weyl's Methods' of Organic Chemistry*, ed. D. Klamann, Georg Thieme Verlag, Stuttgart, 1991, vol. E12b.
58 F. O. Rice and A. L. Glasebrook, *J. Am. Chem. Soc.*, 1934, **56**, 2472.
59 H. B. Singh and P. K. Khanna, *J. Organomet. Chem.*, 1988, **338**, 9.
60 G. Wang, L. Endicott and C. Uher, *Sci. Adv. Mater.*, 2011, **3**, 539.
61 Y. Takagaki, B. Jenichen, U. Jahn, Y. Manzke, M. Ramsteiner and K.-J. Friedland, *Semicond. Sci. Technol.*, 2013, **28**, 025012.
62 A. Koma, K. Sunouchi and T. MiyaJima, *Microelectron. Eng.*, 1984, **2**, 129; O. Lang, R. Schlaf, Y. Tomm,

C. Pettenkofer and W. Jägermann, *J. Appl. Phys.*, 1994, **75**, 7805.
63 Y. Takagaki, B. Jenichen, U. Jahn, M. Ramsteiner, K.-J. Friedland and J. Lähnemann, *Semicond. Sci. Technol.*, 2011, **26**, 125009.
64 N. Periano, M. Winkler, Z. Aabdin, J. Koenig, H. Böttner and O. Eibl, *Phys. Status Solidi A*, 2012, **209**, 289.
65 K. M. F. Shahil, M. Z. Hossain, V. Goyal and A. A. Balandin, *J. Appl. Phys.*, 2012, **111**, 054305.
66 Y. Jiang, Y. Y. Sun, M. Chen, Y. Wang, Z. Li, C. Song, K. He, L. Wang, X. Chen, Q.-K. Xue, X. Ma and S. B. Zhang, *Phys. Rev. Lett.*, 2012, **108**, 066809.
67 W. Richter, H. Köhler and C. R. Becker, *Phys. Status Solidi B*, 1977, **84**, 619.
68 B. Aboulfarah, D. Sayah, A. Mzerd, A. Giani and A. Boyer, *Moroccan J. Condens. Matter*, 2000, **3**, 76.
69 L. W. da Silva, M. Kaviany and C. Uher, *J. Appl. Phys.*, 2005, **97**, 114903.
70 B. Huang, C. Lawrence, A. Gross, G.-S. Hwang, N. Ghafouri, S.-W. Lee, H. Kim, C.-P. Li, C. Uher, K. Najafi and M. Kaviany, *J. Appl. Phys.*, 2008, **104**, 113710.
71 M. R. Scholz, J. Sánchez-Barriga, D. Marchenko, A. Varykhalov, A. Volykhov, L. V. Yashina and O. Rader, *Phys. Rev. Lett.*, 2012, **108**, 256810.
72 L. Plucinski, A. Herdt, S. Fahrendorf, G. Bihlmayer, G. Mussler, S. Döring, J. Kampmeier, F. Matthes, D. E. Bürgler, D. Grützmacher, S. Blügel and C. M. Schneider, *J. Appl. Phys.*, 2013, **113**, 053706.
73 D. Hsieh, Y. Xia, D. Qian, L. Wray, F. Meier, J. H. Dil, J. Osterwalder, L. Patthey, A. V. Fedorov, H. Lin, A. Bansil, D. Grauer, Y. S. Hor, R. J. Cava and M. H. Hasan, *Phys. Rev. Lett.*, 2009, **103**, 146401.
74 *Angle Resolved Photoemission*, ed. S. D. Kevan, Elsevier, Amsterdam, 1992.
75 F. M. Smits, *Bell Syst. Tech. J.*, 1958, **37**, 371 (same as BT Monograph, 3894, Part 2).